Research in Astron. Astrophys. **2012** Vol. **12** No. **4**, 369–382
http://www.raa-journal.org *http://www.iop.org/journals/raa*

***R**esearch in*
***A**stronomy and*
***A**strophysics*

Discovery of Balmer broad absorption lines in the quasar LBQS 1206+1052 *

Tuo Ji[1,2], Ting-Gui Wang[1,2], Hong-Yan Zhou[1,2,3] and Hui-Yuan Wang[1,2]

[1] Key Laboratory for Research in Galaxies and Cosmology, University of Science and Technology of China (USTC), Hefei 230026, China; *tji@mail.ustc.edu.cn*
[2] Center for Astrophysics, USTC, Hefei 230026, China
[3] Polar Research Institute of China, Shanghai 200136, China

Received 2011 October 15; accepted 2012 January 2

Abstract We report the discovery of Balmer broad absorption lines (BALs) in the quasar LBQS 1206+1052 and present a detailed analysis of the peculiar absorption line spectrum. Besides the Mg II $\lambda\lambda 2796,\ 2803$ doublet, BALs are also detected in the He I* multiplet at $\lambda\lambda 2946,\ 3189,\ 3889$ Å arising from the metastable helium 2^3S level, and in Hα and Hβ from the excited hydrogen H I* $n = 2$ level, which are rarely seen in quasar spectra. We identify two components in the BAL troughs of $\Delta v \sim$2000 km s^{-1} width: One component shows an identical profile in H I*, He I* and Mg II with its centroid blueshifted by $-v_{\rm c} \approx 726$ km s^{-1}. The other component is detected in He I* and Mg II with $-v_{\rm c} \approx 1412$ km s^{-1}. We estimate the column densities of H I*, He I*, and Mg II, and compare them with possible level population mechanisms. Our results favor the scenario that the Balmer BALs originate in a partially ionized region with a column density of $N_{\rm H} \sim 10^{21} - 10^{22}$ cm^{-2} for an electron density of $n_{\rm e} \sim 10^6 - 10^8$ cm^{-3} via Lyα resonant scattering pumping. The harsh conditions needed may help to explain the rarity of Balmer absorption line systems in quasar spectra. With an i-band PSF magnitude of 16.50, LBQS 1206+1052 is the brightest Balmer-BAL quasar ever reported. Its high brightness and unique spectral properties make LBQS 1206+1052 a promising candidate for follow-up high-resolution spectroscopy, multi-band observations, and long-term monitoring.

Key words: galaxies: active — quasar: absorption lines — quasar: individual (LBQS 1206+1052)

1 INTRODUCTION

Outflows from active galactic nuclei (AGNs) play an important role in galaxy evolution. Gas in AGNs may be accelerated to high velocities by thermal pressure (Begelman et al. 1983), radiation pressure due to line and continuum absorption (Proga & Kallman 2004), magneto-centrifugal forces (Everett 2005), or their combinations. The outflowing gas is potentially crucial to maintaining the accretion process by carrying away angular momentum; to chemical evolution in AGNs by funneling

∗ Supported by the National Natural Science Foundation of China.

metal-enriched circum nuclear gas into their hosts (Hamann 1999; Wang et al. 2009); and to regulating the co-growth of the black holes and the bulges of their host galaxies by feedback of energy and momentum (e.g. Tremaine et al. 2002; Ferrarese & Merritt 2000), thus quenching the gas supply to the nuclear activity and the host star formation process (e.g. Granato et al. 2004; Di Matteo et al. 2005).

AGN outflows often manifest themselves as blueshifted absorption lines, commonly classified into three categories depending on their width Δv (Hamann & Sabra 2004): (1) broad absorption-lines (BALs) with $\Delta v \gtrsim 2000$ km s^{-1}; (2) narrow absorption lines (NALs) with $\Delta v \lesssim 500$ km s^{-1}; (3) mini-BALs with Δv in between. NALs are very common with a detection rate of about 60% in Seyfert galaxies (Crenshaw et al. 1999) and 50% in quasars (Hamann & Sabra 2004). BALs are seen in $\sim 15\%$ of optically selected quasars[1]. NALs can originate from gas either intrinsic or intervening to AGNs, while BALs are generally believed to be intrinsic to AGNs. All known BAL quasars show high-ionization broad absorption lines (HiBAL), including C IV, Si IV and N V. Besides HiBALs, about 15% of BAL quasars present low-ionization broad absorption-lines (LoBALs), such as Al III, Al II, and Mg II (Weymann et al. 1991; Reichard et al. 2003; Zhang et al. 2010). A minority (another 15%) (Hall et al. 2002) of LoBAL quasars exhibit additional absorption in Fe II and Fe III from both ground and excited levels (FeLoBAL). Even rarer are excited He I* absorption lines, and Balmer absorption lines are extreme rarities.

Only five Balmer-absorption AGNs have been reported thus far: NGC 4151 (Hutchings et al. 2002), SDSS J083942.11+380526.3 (Aoki et al. 2006), SDSS J125942.80+121312.6 (Hall 2007), SDSS J102839.11+450009.4 (Wang et al. 2008), and SDSS J172341.10+555340.5 (Aoki 2010). Three of the five are formally classified as FeLoBALs[2]. The high occurrence rate of both Fe II and Balmer absorption lines indicates that they are closely related, in spite of the small number of such AGNs. Their UV spectra are often profuse in excited Fe II* absorption lines that help to constrain the density of the absorption gas (de Kool et al. 2001). We would like to have a more complete picture of the physical condition and geometry, incorporating the ionization state with He I* as a useful tracer. Interestingly, both NGC 4151 (Hutchings et al. 2002) and SDSS J102839.11+450009.4 (Wang et al. 2008) show He I* NALs, which are the only Balmer-absorption AGNs with He I* covered by previous spectroscopy with negligible contamination. Note that only a handful of He I* absorption AGNs have been reported in the literature[3]. The co-occurrence of He I* and Balmer absorption lines is again remarkably high.

Balmer absorption lines arise from the absorption by $n = 2$ shell excited hydrogen atoms. The H I* $n = 2$ level could be populated by recombination, collisional excitation and Lyα resonant scattering (Hall 2007; Wang et al. 2008). He I* lines arise from absorption by the metastable level He I* 2^3S with transition probability $A(2^3S, 1^1S) = 1.26 \times 10^{-4}$ s^{-1}. Transitions from 2^3S to different upper levels include He I* $\lambda 10830$ in the infrared (Leighly et al. 2011), $\lambda 3889$ in the optical, and $\lambda\lambda 3189, 2946, 2830, 2764$ in the UV. The population of this level comes from the recombination of He$^+$ ions. Plenty of > 24.6 eV photons are needed to ionize neutral helium, but there should not be too many > 4.8 eV photons to ionize He I* 2^3S. A diffuse stellar background provides too many photons to ionize the He I* 2^3S level, and thus these lines are not easily seen in the interstellar medium. We can therefore safely associate the incidence of a neutral helium line with an AGN environment (Rudy et al. 1985). Ignoring second-order effects, recombinations of He$^+$ to

[1] The frequency depends on the specific quasar samples and different BAL selection techniques, ranging from 10% to 40% (e.g. Tolea et al. 2002; Reichard et al. 2003; Trump et al. 2006; Gibson et al. 2009; Ganguly & Brotherton 2008).

[2] The two non-FeLoBALs are NGC 4151 and SDSS J102839.11+450009.4. The former shows Fe II NALs (Hutchings et al. 2002), and Fe II NALs are marginally detected in the later (Wang et al. 2008).

[3] Previously known He I* absorption AGNs include Mrk 231 (Boksenberg et al. 1977; Rudy et al. 1985), NGC 4151 (Hutchings et al. 2002; Anderson 1974), and Q 2359–1241 (Arav et al. 2001). Wang et al. (2008) reported SDSS J102839.11+450009.4 as a remarkably strong narrow Fe II emission-line quasar with He I* $\lambda\lambda$3889, 3189, 2796 narrow absorption lines. Recently, Leighly et al. (2011) reported the first observation of the infrared line He I* $\lambda 10830$, which is 23 times stronger than the optical He I* $\lambda 3889$ and the 10830 line could be used to determine a much lower column density.

He I* 2^3S are mainly balanced with collisional de-excitation of this level (Arav et al. 2001). Upon that, He I* lines can be used to set a lower limit on the He^+ column density, or a lower limit to H II column density with an assumed abundance.

Potentially we could have a good chance to explore the properties of the AGN Balmer absorption line region (ALR). Due to their rarity, however, it is not yet clear whether AGNs with a Balmer ALR form an unusual class, or they are otherwise normal AGNs with our line-of-sight (LOS) happening to penetrate the Balmer ALR, which exists in most if not all AGNs, but with an extremely small global covering factor (GCF). It is not even known how rare Balmer-absorption AGNs are. Discoveries of more such AGNs are obviously helpful in understanding their intriguing nature.

In this paper, we report the new identification of Balmer BALs in LBQS 1206+1052, which was identified during the large bright quasar survey (Hewett et al. 1995) and was recently classified as a LoBAL (Gibson et al. 2009). It is in fact one of ~ 20 Balmer-absorption quasars we recently identified during our systematic search in the quasar catalog from the seventh data release (Schneider et al. 2010) of the Sloan Digital Sky Survey (SDSS, York et al. 2000). With an i band PSF magnitude of 16.50, the high brightness of LBQS 1206+1052 makes it an excellent candidate for a high resolution spectroscopic follow-up and for a long-term variability campaign, which are crucial for absorption line studies. The paper is organized as follows. In Section 2, we analyze the SDSS spectrum and measure column densities of H I*, He I*, and Mg II. The results are discussed in Section 3. Section 4 is a brief summary of our main conclusions.

2 SDSS SPECTROSCOPY

2.1 Continuum and Emission Line Spectrum

LBQS 1206+1052 was targeted as a quasar candidate for spectroscopy, and was observed by the SDSS 2.5m telescope on 2003–03–24 with an exposure time of 3165 seconds. It is very bright with optical PSF magnitudes of 17.19, 16.63, 16.50, 16.34 and 15.92 at u, g, r, i and z bands respectively. The SDSS spectrum, retrieved from the SDSS Data Release 7 database, is corrected for a Galactic reddening of $E(B-V) = 0.023$ mag (Schlegel et al. 1998), and brought to the source rest-frame for further analysis with the systemic redshift ($z = 0.3947 \pm 0.0008$), re-measured from [O III] $\lambda 5007$ as described below. The spectrum is shown in Figure 1. In the rest wavelength range of $\lambda \sim 2500 - 6600$ Å, BALs are evident in Hα, Hβ, He I* $\lambda\lambda$3889, 3189, 2946, and Mg II $\lambda\lambda$2796, 2803 with a velocity range of $\Delta v \sim 0 - 2000$ km s^{-1}.

Proper modeling of continuum and emission lines is essential to derive absorption line parameters. In the observed quasar spectrum, prominent broad and narrow emission lines are siting on top of a pseudo-continuum, consisting of thermal emission from the accretion disk, a Balmer continuum from the broad line region or disk, the blended FeII lines and high order Balmer lines. We fit the pseudo-continuum and emission lines in two steps as follows. In the first step, the pseudo-continuum is modeled with three components: a single power law to mimic emission from the accretion disk, a Balmer continuum plus high order Balmer lines, and blended Fe II emission lines.

Following Dietrich et al. (2003) and Tsuzuki et al. (2006), the Balmer continuum is expressed by

$$F_\lambda = F_{3646} \times B_\lambda(T_\mathrm{e})(1 - \mathrm{e}^{-\tau_\lambda}) \qquad \text{for } \lambda \leq 3646\,\text{Å}\,,$$

where F_{3646} is the normalization coefficient at Balmer edge 3646 Å and $\tau_\lambda = \tau_\mathrm{BE}(\lambda/\lambda_\mathrm{BE})^3$ in which τ_BE is optical depth at Balmer edge λ_BE (3646 Å), and $B_\lambda(T_\mathrm{e})$ is the Planck function at an electron temperature T_e, which is assumed to be 15 000 K (Dietrich et al. 2003). High order Balmer lines up to $n = 50$ are also used in the fit. Relative strengths of these lines are fixed using the line emissivities for Case B, $T_\mathrm{e} = 15\,000$ K and $n_\mathrm{e} = 10^8$ cm^{-3} as calculated by Storey & Hummer (1995), and each line is assumed to have a Gaussian profile with an FWHM of 3000 km s^{-1}. The relative flux of the high order Balmer lines to the flux of the Balmer continuum at the edge is fixed

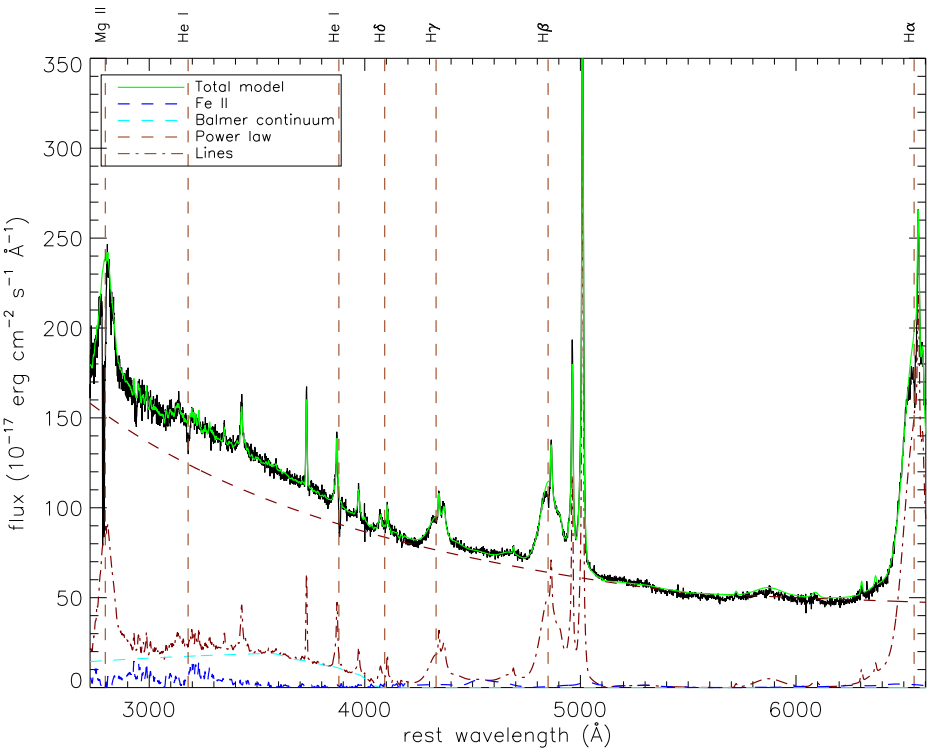

Fig. 1 SDSS spectrum of LBQS 1206+1052. Prominent absorption features are marked as vertical dashed lines and labeled on the top. Model fits to the spectrum are shown as green lines. Different components of the spectral model are also shown.

using the results in Wills et al. (1985). Thus these blended high order Balmer lines and the Balmer continuum join smoothly, forming a pseudo-continuum (Wills et al. 1985). Note that none of the assumptions concerning the Balmer continuum and high order Balmer lines will have a significant effect on the measurement of absorption lines because all these features are quite broad.

The optical and UV Fe II emissions are modeled separately with broadened empirical templates derived from observed quasar spectra. For the optical band long-ward of 3500 Å, we use a template extracted from the optical spectrum of proto-type narrow line Seyfert 1 galaxy I Zw 1 (Véron-Cetty et al. (2004)). The template includes both the broad and narrow component, and the latter also includes transitions from Ni II, Cr II and Ti II. For the UV portion short-ward of 3500 Å, we employ a template built from SDSS J1632+3405 (Zhou et al. 2012 in preparation). SDSS J1632+3405 has ultra strong UV Fe II emission, which has an FWHM of 400 km s^{-1}, only about half of that in I Zw 1. The narrow width makes it easy to separate Fe II multiplets from the other lines and also among different multiplets. Thus it is a more promising target for building a UV Fe II template. The relative strength of different UV multiplet ratios are allowed to vary during the fit. This is a common technique when modeling quasar Fe II spectra (Tsuzuki et al. 2006; Kovačević et al. 2010; Sameshima et al. 2011).

The above continuum components are combined to fit the SDSS spectrum in the following windows: 2855–3010, 3625–3645, 4170–4260, 4430–4770, 5080–5550, and 6050–6200 Å, which are devoid of strong emission lines (Vestergaard & Wilkes 2001). The window 3625–3645 is used

to constrain the Balmer continuum. The best fitted parameters are derived by minimization of χ^2. The line spectrum is then acquired by subtracting the best fitted pseudo-continuum from the original spectrum.

In the second step, emission-lines are measured in this line spectrum. All narrow lines or narrow components of broad lines except [O III] and [Ne III] are fitted with a single Gaussian. The centroids of the Gaussian are fixed to the vacuum wavelengths of these lines, and their widths are tied during the fit. [O III] and [Ne III] show an additional blueshifted component, and are fitted with two Gaussians for each multiplet. The width and velocity shift between the two Gaussians are tied for these lines during the fit, while their normalizations are allowed to vary independently. The [Ne III] λ3869 emission line is affected by He I* λ3889 absorption, and the pixels affected by the He I* λ3889 line are masked during the fit according to the corresponding He I* λ3189 absorption profile. Narrow lines included in this fit are [Ne V] λ3425, [O II], [Ne III] λ3869, Hδ, Hγ, [O III] λ4363, He II λ4686, Hβ, [O III] $\lambda\lambda$4959, 5007, [O I] $\lambda\lambda$6300, 6364, Hα, and [N II] $\lambda\lambda$6548, 6583.

Broad lines are fitted using as many Gaussians as are statistically justified. The broad component of Hβ is fitted with 4 G, while Hα is fitted with 3 G because the red part of the Hα line is not in the observed spectrum range. Pixels affected by Balmer absorption are masked as done for He I* λ3889. The fitted profiles of broad Hα and Hβ lines are very similar in the overlapping portion of the velocity space, lending credit to our fitting scheme of broad lines. Mg II lines are fitted with two Gaussians in the same way as for Balmer lines except that no narrow Gaussian is used because there is no explicit narrow Mg II doublet.

The best fit model is overlaid in Figure 1, together with individual components.

2.2 Absorption Line Spectrum and Column Densities

We use the best fit model to normalize the absorption line spectrum. We first subtract model narrow emission lines from the observed spectrum before normalization, since the absorption gas does not cover the narrow emission line region (NLR) in all well studied BAL quasars. The Mg II doublet and Balmer absorption lines are superposed on top of broad emission lines. They should be normalized in different ways depending on whether the absorbing gas covers the broad emission line regions (BLR) or not (de Kool et al. 2001): (1) The observed data should be divided by the sum of the continuum and broad emission lines if it does. (2) If not, the broad emission lines should be subtracted before the observed data are normalized by the continuum. We adopt the second normalization scheme because of the following hints.

We enlarge Figure 1 and display the close-ups in Figure 2 focusing on the two Hα and Mg II regimes. It can be seen clearly that the modeled broad emission lines just brush the tip of the BAL trough in both the Hα and Mg II lines. This can be most naturally interpreted in the second scheme with an optical depth $\tau \gg 1$ at the centroid of both Hα and Mg II BAL troughs. Otherwise we would need to have two coincidences at once, which is unlikely if not impossible. The interpretation is also consistent with the marginal detection of Ca II K in absorption, which suggests a large optical depth in the Mg II BAL doublet for any reasonable abundance.

The normalized absorption line spectrum is shown in Figure 3, and the apparent optical depth profile of the Mg II $\lambda\lambda$2796, 2803 doublet is shown in Figure 4. The normalized flux at the line centroid approaches zero for Mg II and Hα lines. Note that Balmer emission line profiles at the absorption line position are somewhat uncertain due to a lack of independent constraint. We use a 1-σ error of normalized flux to deduce a lower limit for the apparent optical depth of the deepest pixels. The Mg II profile apparently shows two components, one broad component with corresponding Balmer and helium absorption lines. The other one is relatively narrow and shows He I* lines, possibly the Ca II λ3934 absorption line and a little Balmer absorption line. We simultaneously fit the apparent optical depth $\tau(v)$ of all absorption lines with two Lorentzians for each line, which are similar to Voigt profiles for small b values. The line centroid of other lines are tied to that of Mg II

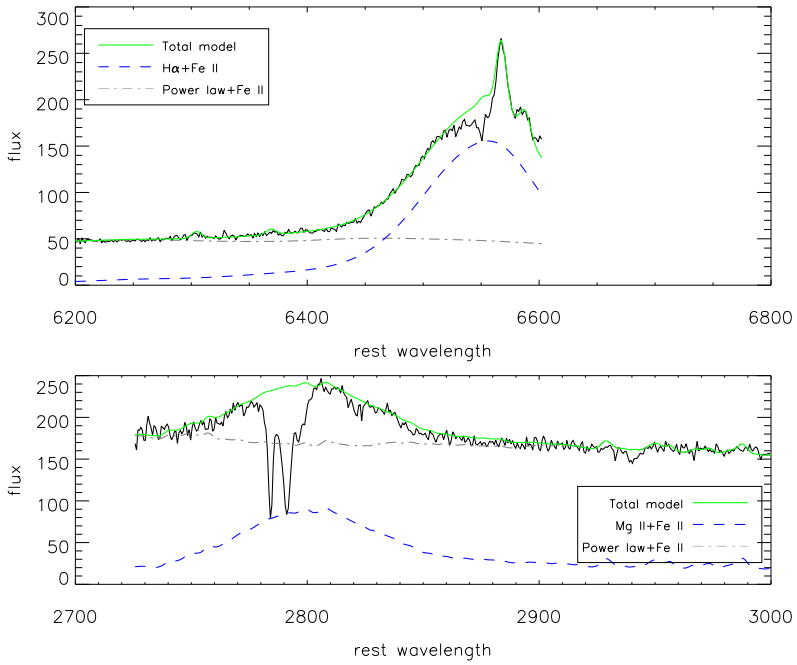

Fig. 2 Close-ups of Fig. 1 enlarged in the Hα (*upper*) and Mg II (*lower*) regimes.

Table 1 Absorption Line Parameters

Line	Wavelength(Å)	f_{ij} [a]	W_λ(C1)[b]	W_λ(C2)[c]
Hα	6564.41	0.6400	27.88 ± 2.16	< 0.70
Hβ	4862.68	0.1190	3.41 ± 0.25	0.15 ± 0.08
Hγ	4341.68	0.0446	0.46 ± 0.13	none
He I* 3889	3889.75	0.0278	3.35 ± 0.19	0.47 ± 0.08
He I* 3189	3188.66	0.0110	1.46 ± 0.13	0.19 ± 0.06
He I* 2946	2945.96	0.0053	0.91 ± 0.13	0.15 ± 0.06
Mg II 2796	2796.35	0.6160	6.00 ± 0.31	7.29 ± 0.73
Mg II 2803	2803.53	0.3060	3.01 ± 0.15	7.31 ± 0.73
Ca II 3934	3934.78	0.6270	none	< 0.24

a: Oscillator strengths are from NIST Atomic Spectra Database (*http://physics.nist.gov/PhysRefData/ASD/*).
b: Equivalent widths for component 1, which is a Gaussian with centroid at –726 km s^{-1} and FWHM 603 km s^{-1}.
c: Equivalent widths for component 2, which is a Gaussian with centroid at –1412 km s^{-1} and FWHM 208 km s^{-1}.

lines and the line width is assumed to be equal for the same component during the fit. The best fitted model for Mg II is also shown in Figure 4, and overlaid in Figure 3. The fitted EWs for each line are shown in Table 1. The low velocity component is centered at -726 km s^{-1} and with an FWHM of 603 km s^{-1}, it is referred to as component 1 (C1) hereafter, while a high velocity component with a line centroid of -1412 km s^{-1} and an FWHM of 208 km s^{-1} is referred to as component 2 (C2) hereafter.

The C1 component shows similar profiles in Mg II, He I* and Balmer absorption lines. There is only one pixel in the Hα line that is inconsistent with our model, which can be attributed to imperfect emission line modeling. The τ ratio of 2796 to 2803 for C1 is 2:1, which is consistent with that of the

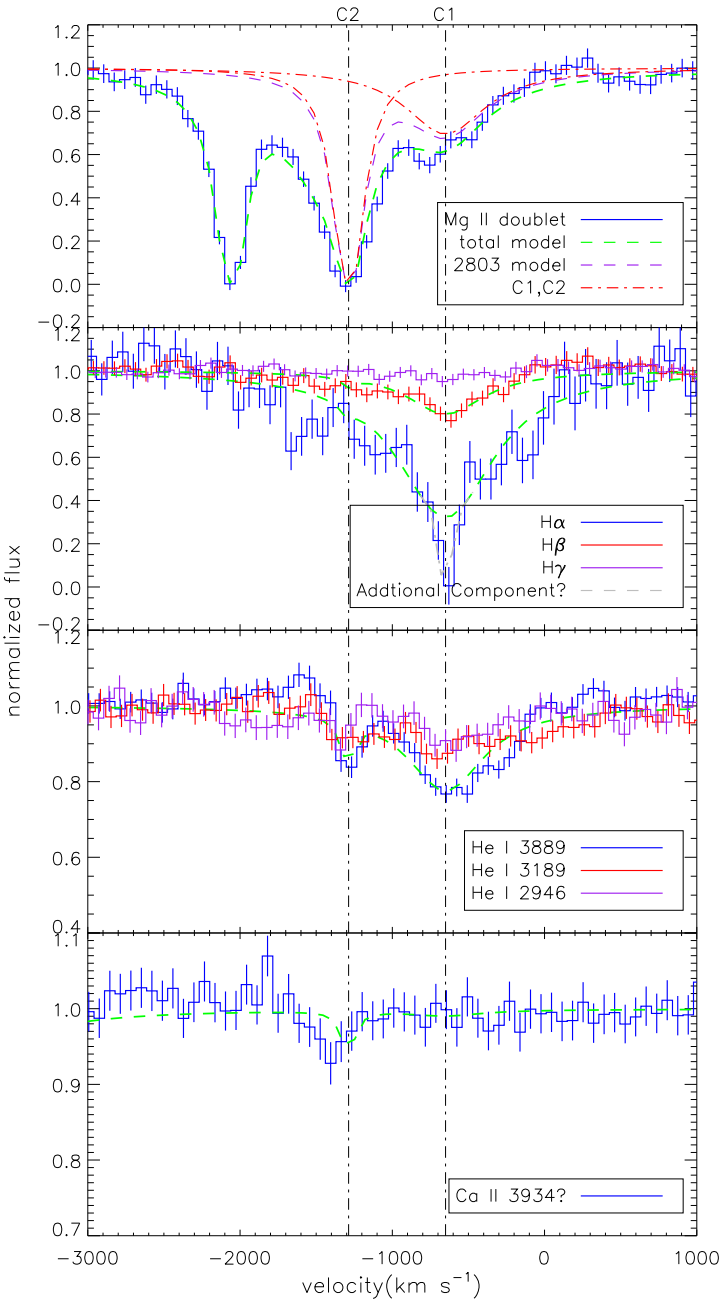

Fig. 3 Normalized intensity assuming that the absorption gas only covers the continuum source and not the BLR. From top to bottom are Mg II λ 2803, Balmer absorption lines and He I* absorption lines, and Ca II λ3934. Different lines are plotted using different colors as indicated by legends on the lower right of each panel. Best fitted models of absorption profiles are shown as green lines, and only fits for Mg II, Hα, He I* λ3889 and Ca II λ3934 are shown for clarity. The two components are shown in red dot-dashed lines for the Mg II fit, whose centers are marked as black vertical lines. The absorption model is oversimplified as judged by the central pixels of the Hα line, but it has little effect on our analysis.

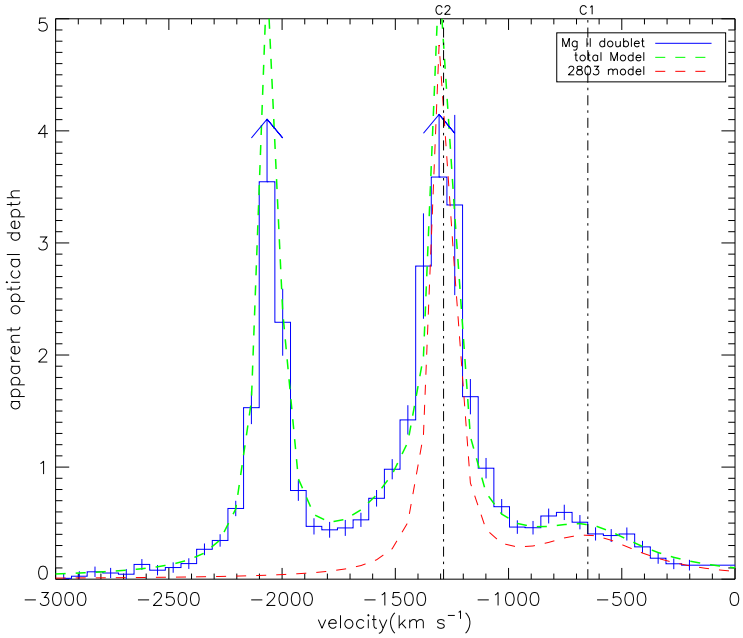

Fig. 4 Apparent optical depth for the Mg II $\lambda\lambda$2796, 2803 doublet as a function of velocity relative to the rest-frame 2803 Å. The pixels marked as up-arrows are the lower limits of optical depth values. These pixels have a normalized flux approaching zero and the 1-σ errors of normalized flux are used to get the optical depth limit. Various components are also plotted using different lines and colors as indicated by legends.

absorption gas fully covering the continuum source. To check this, we compare the ratios of Balmer lines with their theoretical values. From Table 1, we can see that the Balmer absorption line EW ratio $\mathrm{EW(H}\alpha) : \mathrm{EW(H}\beta) = 8.19^{+1.29}_{-1.17}$ is consistent with the theoretical $f\lambda$ ratio 7.26, thus we favor the situation where the absorbing gas of C1 fully covers the continuum source and the lines are not saturated. Under this assumption, we derive column densities of various ions from their equivalent widths W_λ, using the equation from Jenkins (1986)

$$N = \frac{m_\mathrm{e}c^2}{\pi \mathrm{e}^2 f\lambda^2} W_\lambda. \tag{1}$$

We get a column density for Mg II from the Mg II λ2803 line $N_{\mathrm{Mg^+}} = (1.41 \pm 0.07) \times 10^{14}$ cm^{-2}, for hydrogen at $n = 2$ from the Hβ line $N_\mathrm{H}(n = 2) = (1.37 \pm 0.10) \times 10^{14}$ cm^{-2} and for helium from the He I* λ3889 line $N_{\mathrm{He\ I}\ 2^3S} = (8.99 \pm 0.50) \times 10^{14}$ cm^{-2}.

Component C2 shows a consistent absorption trough in Mg II and He I*. A weak line near 3930 Å may be attributed to the Ca II K absorption line of this component (blueshifted by 100 km s^{-1} relative to other lines). The Mg II absorption line is seriously saturated as indicated by the doublet ratio of Mg II, $\mathrm{EW}_{2796}/\mathrm{EW}_{2803} \sim 1$. Thus we can only get a lower limit of the Mg II column density using Equation (1), $N_{\mathrm{Mg^+}} > (3.43 \pm 0.34) \times 10^{14}$ cm^{-2}. Alternatively, we may integrate the apparent optical depth profile $N = \frac{m_\mathrm{e}c^2}{\pi e^2 f\lambda^2} \int \tau_v \, dv$ and obtain a column density of $N_{\mathrm{Mg^+}} = (5.84 \pm 0.45) \times 10^{15}$ cm^{-2}, which is likely to be close to the real value. The Hα line of C2 is not detected significantly. We derive an upper limit on its column density

$N_{\rm H^0}(n=2) < 9\times10^{12}$ cm^{-2}. The He I* lines in this component are generally weak; we find a column density of $N_{\rm He\ I\ 2^3S} = (1.25\pm0.22)\times10^{14}$ cm^{-2}.

3 DISCUSSION

The overall rarity of Balmer absorption line quasars indicates that either the conditions for outflowing gas to maintain a sufficient population of $n=2$ level hydrogen atoms must be very harsh. We will discuss the conditions required to produce the Balmer absorption lines in C1 with different mechanisms.

If the $n=2$ level hydrogen atoms of this component are caused by collisional excitation, they must exist in the H I region or probably the partially ionized region. The observed Mg II absorption lines suggest that there is a partially ionized absorption line region. Mg^+ ions are created by photons with energy greater than 7.6 eV and destroyed by photons with energy greater than 15.0 eV, thus they mainly survive in the outer part of the H II region and mostly in the partially ionized region. Assuming that Mg^+ is the dominant species of Mg and there is a solar abundance with $[{\rm Mg/H}] = -4.4$, we get a lower limit on the total hydrogen column density of 3.54×10^{18} cm^{-2} for the partially ionized zone. If thermal equilibrium is achieved, then using Boltzmann's equation: $n_2/n_1 = 4{\rm exp}(-10.2\ {\rm eV}/kT)$, in which n_1 and n_2 are densities of $n=1$ and $n=2$ level hydrogen, one readily yields a column density of $n=2$ hydrogen of 6.8×10^{13} cm^{-2}, which is close to the observed hydrogen column density $(1.37\pm0.10)\times10^{14}$ cm^{-2}, at a typical temperature T$\sim 10^4$K for photo-ionized gas. However, thermal equilibrium requires that collisions with thermal particles are the dominant process for excitation and de-excitation. This yields a lower density limit

$$n_c = A_{21}/[q_{21}(1+\tau_{0l})] = 8.7\times10^{16}/(1+\tau_{0l}){\rm cm}^{-3}$$

accounting for the resonant scattering of Lyα photons, where τ_{0l} is the optical depth of Lyα from the center of the region. For a gaussian distribution of turbulence, we can write

$$\tau_{0l} \simeq 7.6\times10^6 b_3^{-1} N_{\rm H^0,22} \sim 10^3\,,$$

where $b_3\sim1$ is the turbulent velocity of gas in units of 10^3 km s^{-1} and $N_{\rm H^0,22}$ the neutral hydrogen column density in 10^{22} cm^{-2}. This gives a density too high for any reasonable line absorbing gas.

When the density is lower than the critical density discussed above, a detailed equilibrium of the $n=2$ level must be considered. Transition of the $2s$ state to the ground level is forbidden with a small Einstein coefficient $A = 8.23\ {\rm s}^{-1}$ via a 2-photon process, while transition from $2p$ to $1s$ is allowed. The two levels have very different excitation processes, therefore, we will consider them separately in the following analysis.

Let us first consider the equilibrium of the $2p$ level. In the case that absorption gas is optically thin to Lyα, the equilibrium between recombination to $n=2$ and radiative decay from $2p$ to $2s$ yields $n_{2p}/n_{\rm H^+} = \alpha_{\rm eff} n_{\rm e}/A_{2p,2s}$[4]. However, the gas is likely to be very optically thick to Lyα. In this case, each Lyα photon is scattered $1+\tau_{0l}$ times on average before escaping (Osterbrock & Ferland 2006). This leads to the $2p$ population being larger by a factor of $1+\tau_{0l}$ than the above optically thin equation, i.e.

$$n_{2p}/n_{\rm H^+} \simeq \tau_{0l}\alpha_{\rm eff} n_{\rm e}/A_{2p,2s} \simeq 7.3\times10^{-9} n_{\rm e,6} N_{\rm H^0,22} b_3^{-1}.$$

To get the observed $n=2$ column density, we require

$$N_{\rm H,22} \simeq 1.4 f_{\rm H^+}^{-1}(1-f_{\rm H^+})^{-1/2} b_3^{1/2} n_{\rm H,6}^{-1/2} (N_{n=2}/1.4\times10^{14}\ {\rm cm}^{-2})^{1/2}, \quad (2)$$

[4] As we discuss next, the absorbing gas is probably in the partially ionized region, where the typical temperature is significantly lower than 10^4 K, and $q_{1s\rightarrow2p} \propto \exp(-\frac{\Delta E}{kT}) \ll \alpha_{\rm eff}$ in this region, thus we ignore the collisional excitation of the 2p level here.

where $f_{\rm H^+}$ is the fraction of ionized hydrogen. As discussed in Section 2.2, it is very likely that the BALR in LBQS 1206+1052 fully covers the accretion disk but does not cover the BLR. This suggests

$$10^{14}\,{\rm cm} \sim r_{\rm AD} < r_{\rm BALR} \ll r_{\rm BLR} \sim 10^{17}\,{\rm cm}\,,$$

where $r_{\rm AD}$, $r_{\rm BALR}$ and $r_{\rm BLR}$ are the size of the accretion disk, the broad absorption line region, and the broad emission line region, respectively. We infer a hydrogen column density of $N_{\rm H} \sim 10^{21} - 10^{22}$ cm^{-2} of the partially ionized gas for an electron density of $n_{\rm H} \sim 10^6 - 10^8$ cm^{-3}. For a higher $n_{\rm H}$ and lower $N_{\rm H}$, the BALR would not be large enough to fully cover the accretion disk, while the BALR would be large enough to cover the BLR for a lower $n_{\rm H}$ and higher $N_{\rm H}$. The inferred $N_{\rm H}$ value is much larger than the thermal equilibrium value.

Next, we consider the population in the $2s$ level. The equilibrium equation of the $2s$ level can be written as

$$n_{\rm e} n_{\rm H^+} \alpha_{{\rm eff},2s} + n_{\rm H} n_{\rm e} q_{1s\rightarrow 2s} = n_{2s}\left[A_{21} + n_{\rm e}(q_{2s\rightarrow 2p} + q_{2s\rightarrow nl}) + \int_{\nu_1}^{\infty} \frac{\alpha_\nu L_\nu}{4\pi r^2 h\nu} d\nu\right], \qquad (3)$$

in which we ignored the effect of the $2p$ level for the time being[5]. The first term on the left hand side represents recombination to the $2s$ level, while the second term represents collisional excitation. Given that $\alpha_{{\rm eff},2s}$ and $q_{1s\rightarrow 2s}$ are on the same order of magnitude ($\alpha_{{\rm eff},2s} = 0.838 \times 10^{-13}$ cm^{-3} s^{-1}, $q_{1s\rightarrow 2s} = 1.67 \times 10^{-13}$ cm^{-3} s^{-1} at $T = 10\,000$ K), the ratio of the first to second term is mainly determined by the ratio of $n_{\rm H^+}$ to $n_{\rm H}$. In the H II region where $n_{\rm H^+}/n_{\rm H}$ is high, the recombination mechanism dominates the population of the $n = 2$ level, while in the H I region or PIZ where $n_{\rm H^+}/n_{\rm H}$ is low, the collisional excitation dominates the population of the $n = 2$ level, we treat them separately.

In the H I or PIZ region, we ignore the first term on the left hand side of Equation (3). The third term on the right hand side is the photoionization of the $n = 2$ level, in which ν_1 is the frequency at Balmer edge $\lambda = 3646$ Å. It can be shown that the third term is negligible by substituting the integration term with

$$U = \int_{\nu_0}^{\infty} L_\nu/(4\pi r^2 c n_{\rm H} h\nu) d\nu$$

and $\nu_0 = 4\nu_1$ and assuming a power law index of the optical-UV continuum $\alpha_\nu = -0.44$ (Vanden Berk et al. 2001). If the density $n_{\rm e}$ of absorption gas is sufficiently low compared to the critical density

$$n_c = A_{2s\rightarrow 1s}/q_{2s\rightarrow 2p} \sim 1.5 \times 10^4\,{\rm cm}^{-3}$$

at $T = 10\,000$ K (Osterbrock & Ferland 2006), the equilibrium gives

$$n_{2S}/n_{\rm H} = n_{\rm e} q_{1s\rightarrow 2s}/A_{2s\rightarrow 1s} \leq q_{1s\rightarrow 2s}/q_{2s\rightarrow 2p}\,,$$

otherwise if the density is moderately high, the second route will dominate, which gives $n_{2S}/n_{\rm e} = q_{1s\rightarrow 2s}/q_{2s\rightarrow 2p}$, which is around 3×10^{-10} at a temperature of $10\,000$ K [6]. This requires a total hydrogen column of greater than 5×10^{23} cm^{-2} to generate the observed Balmer absorption lines' EW in Q 1206+1052. Clearly, collisional excitation is much less efficient in populating the $n = 2$ level than Lyα resonant scattering in partially ionized gas in AGNs if the gas density is high.

Alternatively the $n = 2$ level population could arise from ionized gas via recombination, and we ignore the second term on the left hand side of Equation (3). As in the collisional excitation dominated case, we further distinguish cases when densities are below or above the critical density

[5] Had $2p$ been significantly populated due to Lyα trapping in dense gas as discussed in the last paragraph, because of large collision strength, the $2p$ and $2s$ levels would reach thermal equilibrium, that is n_{2s}: $n_{2p} = 1 : 3$.

[6] Wang et al. (2008) used an incorrect $q_{2s\rightarrow 2p}$ value resulting in an incorrect value of $n_{2S}/n_{\rm H} \sim 0.02$.

10^4 cm^{-3} set by the collisional angular-momentum transition from $2s$ to the $2p$ state. If the density is higher than that, the $2s$ state is populated by recombination and depopulated via collisional excitation to the $2p$ state, which radiatively decays to the $n = 1$ level. The equilibrium gives

$$n_{2s}/n_{\rm H^+} \sim \alpha_{2s}/q_{2s\rightarrow 2p} \sim 0.44 \times 10^{-10}$$

at $T = 10\,000$ K. Otherwise if the density is lower than the critical density, the equilibrium is built through the balance between the two-photon continuum emission of $2s \rightarrow 1s$ and the recombination to the $2s$ state, which gives

$$n_{2s}/n_{\rm H+} \sim n_{\rm e}\alpha_{2s}/A_{2s\rightarrow 1s} \leq \alpha_{2s}/q_{2s\rightarrow 2p} \sim 0.44 \times 10^{-10}\,.$$

The last equation in the above estimations utilizes the fact that when this route dominates the equilibrium,

$$n_{\rm e} \leq n_c = A_{2s\rightarrow 1s}/q_{2s\rightarrow 2p}\,.$$

Thus if indeed the level two population is from the H II zone, the observed $n = 2$ columns require a total hydrogen column of at least 3.1×10^{24} cm^{-2}. The column density appears too large for the absorbing gas.

To summarize, the resonant scattering of Lyα is much more efficient in populating the $n = 2$ level in the partially ionized region if gas density is high. In this case, the column density required to account for the Balmer absorption lines in C1 is in the range 10^{21} to 10^{22} cm^{-2} for a gas density between 10^6 and 10^8 cm^{-3} and decreases with the square root of the gas density. At much lower densities, collisional excitation may take over the resonant scattering pumping, and it requires a column density of at least $5{\times}10^{23}$ cm^{-2}. In the H II region, recombination can lead to the required $n = 2$ level at a very high column density of $N_{\rm H^+} = 5 \times 10^{24}$ cm^{-2}.

A thick H II region is not consistent with the observed helium absorption lines. He I* absorption arises from absorption by the metastable He I* 2^3S state. The equilibrium equation of this level is (Arav et al. 2001)

$$n_{\rm He+}n_{\rm e}\alpha_T = n_{2^3S}\left[A_{21} + n_{\rm e}(q_{2^3S,2^1S} + q_{2^3S,2^1P}) + n_{\rm e}q_{\rm ci} + \int_{\nu_0}^{\infty}\frac{\alpha_\nu L_\nu}{4\pi r^2 h\nu}d\nu\right], \qquad (4)$$

where ν_0 is the threshold frequency at ionization energy 4.77 eV of the 2^3S state, and $q_{2^3S,2^1S}$, $q_{2^3S,2^1P}$ and $q_{\rm ci}$ are corresponding collisional rates. The left hand term represent recombination of He II ions with electrons. On the right hand side of the equation, the first term is radiative transition from 2^3S to 1^1S , which is a forbidden transition and can be neglected; the second term is collisional de-excitation of 2^3S to 2^1S and 2^1P; and the third and forth terms represent collisional and radiative ionization of 2^3S respectively. Neglecting terms other than collisional de-excitation, we get

$$\frac{n_{2^3S}({\rm He}^0)}{n_{\rm He^+}} = \frac{5.8 \times 10^{-6}T_4^{-1.19}}{1 + 3110T_4^{-0.51}n_{\rm e}^{-1}}, \qquad (5)$$

where $T_4 = T/10^4$ K $\simeq 1$ for photoionized gas. At a reasonable gas density, the observed He I* 2^3S column density implies there is a column density of the H II zone of only 10^{21} cm^{-2}. This column density is much lower than required for an excitation of the $n = 2$ level via recombination, but is consistent with Lyα pumping as the main excitation mechanism for the $n = 2$ population.

A thick H I region can produce too large column densities of Mg II. It is shown that the fraction of Mg$^+$ in the PIZ of the AGN ionized region ranges from 10^{-3} cm^{-3} close to the H II-H I transition zone to near dominating species deep inside the H I region. To meet the observed Mg II column density, the PIZ zone cannot be thicker than a few 10^{21} cm^{-2}, which rules out the possibility of collisional excitation without Lyα pumping. Therefore, Lyα pumping remains the only possible

excitation mechanism, at least for the Balmer absorption in this object, and the density is likely to be higher than 10^8 cm^{-3}.

For C2, Mg II lines are seriously saturated. The column densities derived from integrated Mg II apparent optical depth profiles set a lower limit on the hydrogen column density of $N_{\rm H} = 6.23 \times 10^{19}$ cm^{-2}. On the other hand, a lower limit of the column density ($N_{\rm H} \sim 10^{21}$ cm^{-2}) can be derived from the He I* absorption lines with an analysis similar to that for C2. Although the Mg II column density is much larger than that of C1 and the He I* column density is similar, the Balmer absorption is not detected with an upper limit of 9×10^{12} cm^{-2}.

As discussed above, $n = 2$ hydrogen is populated much more efficiently via the Lyα pumping process than by other routes. The process works well in relatively dense material and in a partially ionized medium. Lack of Balmer absorption lines can be attributed to any of the following cases: the total column density of the partially ionized zone is too low; the ionization of the gas may be too large; the density of gas is too low, or any combination of the three. As pointed out in Lu et al. (2008), a trace amount of Mg^+ may originate from an ionized region with log $U \geq -1.5$ where Al^{2+} and C^{3+} live. A total hydrogen column density of $N_{\rm H} \sim 10^{22}$ cm^{-2} is required to generate the observed Mg^+ if this is the case, although the column density is much larger than the lower limit set by helium absorption, and we cannot rule out this possibility for now.

4 SUMMARY AND FUTURE PROSPECTIVES

We present a detailed analysis of absorption line systems in the quasar LBQS 1206+1052, the brightest quasar showing Balmer absorption lines Hα and Hβ. From its medium resolution SDSS spectrum, we found that there are mainly two absorption components. Component 1 is blueshifted by -726 km s^{-1} and has an FWHM of 603 km s^{-1}, showing corresponding absorption in Balmer, He I* and Mg II. This component has full coverage of the continuum source but not the BLR. Component 2 is blueshifted by –1412 km s^{-1} and has an FWHM of 207 km s^{-1}. The Mg II lines are seriously saturated for this component, while helium lines are generally too weak to facilitate partial coverage analysis and Balmer absorption lines are not detected. If the H$(n = 2)$ is the outcome of recombination, a typical ionized hydrogen column density of several 10^{24} cm^{-2} is needed to generate the observed absorption in the Balmer series. Collisional excitation of the $2s$ level without Lyα resonance scattering in play also requires a column density as high as 5×10^{23} cm^{-2}. These column densities are inconsistent with either Mg II or He I* absorption lines. Thus, Lyα scattering in a partially ionized region is the main mechanism of populating $n = 2$ level hydrogen, and the required column density is 10^{21} to 10^{22} cm^{-2} for a gas density between 10^6 to 10^8 cm^{-3} and decreases with the square root of the gas density. These harsh conditions required, i.e. the large column density and gas density, may help to explain the overall rare population of such objects, only ~ 20 (Ji et al. 2011 in preparation) out of 105 783 DR7 quasars (Schneider et al. 2010).

Due to the medium S/N and resolution of an SDSS spectrum, we cannot elaborate further about the nature of the absorber. However, the bright magnitudes make LBQS 1206+1052 the most promising candidate for high resolution spectroscopic observation, which will provide a resolved velocity profile for pixel-to-pixel based covering factor and velocity structure analysis. The Earth's atmosphere cutoff wavelength of 3200 Å corresponds to a rest-frame wavelength of 2285 Å at $z = 0.4$ of the quasar. Given the high rate of detecting Balmer absorption in FeLoBALs, we expect to detect absorption lines in the UV1 multiplet arising from excited levels of Fe II ions from ground-based facilities, such as Keck and MMT, which may help to determine the density of the absorption gas (Korista et al. 2008). A long-term monitoring campaign is also helpful to explore its physical/geometrical properties.

Acknowledgements This work is supported by the National Natural Science Foundation of China (Grants Nos. 10973013 and 11033007), and the Fundamental Research Funds for the Central

Universities through grant WK 2030220006, and the SOA project CHINARE2012–02–03. This paper has made use of data from NED, NIST and SDSS. Funding for the SDSS and SDSS-II has been provided by the Alfred P. Sloan Foundation, the Participating Institutions, the National Science Foundation, the U.S. Department of Energy, the National Aeronautics and Space Administration, the Japanese Monbukagakusho, the Max Planck Society, and the Higher Education Funding Council for England. The SDSS Web Site is *http://www.sdss.org/*. The SDSS is managed by the Astrophysical Research Consortium for the Participating Institutions. The Participating Institutions are the American Museum of Natural History, Astrophysical Institute Potsdam, University of Basel, University of Cambridge, Case Western Reserve University, University of Chicago, Drexel University, Fermilab, the Institute for Advanced Study, the Japan Participation Group, Johns Hopkins University, the Joint Institute for Nuclear Astrophysics, the Kavli Institute for Particle Astrophysics and Cosmology, the Korean Scientist Group, the Chinese Academy of Sciences (LAMOST), Los Alamos National Laboratory, the Max-Planck-Institute for Astronomy (MPIA), the Max-Planck-Institute for Astrophysics (MPA), New Mexico State University, Ohio State University, University of Pittsburgh, University of Portsmouth, Princeton University, the United States Naval Observatory, and the University of Washington.

References

Anderson, K. S. 1974, ApJ, 189, 195
Aoki, K. 2010, PASJ, 62, 1333
Aoki, K., Iwata, I., Ohta, K., et al. 2006, ApJ, 651, 84
Arav, N., Brotherton, M. S., Becker, R. H., et al. 2001, ApJ, 546, 140
Begelman, M. C., McKee, C. F., & Shields, G. A. 1983, ApJ, 271, 70
Boksenberg, A., Carswell, R. F., Allen, D. A., et al. 1977, MNRAS, 178, 451
Crenshaw, D. M., Kraemer, S. B., Boggess, A., et al. 1999, ApJ, 516, 750
de Kool, M., Arav, N., Becker, R. H., et al. 2001, ApJ, 548, 609
Di Matteo, T., Springel, V., & Hernquist, L. 2005, Nature, 433, 604
Dietrich, M., Hamann, F., Appenzeller, I., & Vestergaard, M. 2003, ApJ, 596, 817
Everett, J. E. 2005, ApJ, 631, 689
Ferrarese, L., & Merritt, D. 2000, ApJ, 539, L9
Ganguly, R., & Brotherton, M. S. 2008, ApJ, 672, 102
Gibson, R. R., Jiang, L., Brandt, W. N., et al. 2009, ApJ, 692, 758
Granato, G. L., De Zotti, G., Silva, L., Bressan, A., & Danese, L. 2004, ApJ, 600, 580
Hall, P. B. 2007, AJ, 133, 1271
Hall, P. B., Anderson, S. F., Strauss, M. A., et al. 2002, ApJS, 141, 267
Hamann, F. 1999, in Astronomical Society of the Pacific Conference Series 175, Structure and Kinematics of Quasar Broad Line Regions, eds. C. M. Gaskell, W. N. Brandt, M. Dietrich, D. Dultzin-Hacyan, & M. Eracleous, 33
Hamann, F., & Sabra, B. 2004, in Astronomical Society of the Pacific Conference Series 311, AGN Physics with the Sloan Digital Sky Survey, eds. G. T. Richards, & P. B. Hall (San Francisco: Astronomical Society of the Pacific), 203
Hewett, P. C., Foltz, C. B., & Chaffee, F. H. 1995, AJ, 109, 1498
Hutchings, J. B., Crenshaw, D. M., Kraemer, S. B., et al. 2002, AJ, 124, 2543
Jenkins, E. B. 1986, ApJ, 304, 739
Korista, K. T., Bautista, M. A., Arav, N., et al. 2008, ApJ, 688, 108
Kovačević, J., Popović, L. Č., & Dimitrijević, M. S. 2010, ApJS, 189, 15
Leighly, K. M., Dietrich, M., & Barber, S. 2011, ApJ, 728, 94
Lu, H., Wang, T., Yuan, W., et al. 2008, ApJ, 680, 858

Osterbrock, D. E., & Ferland, G. J. 2006, Astrophysics of Gaseous Nebulae and Active Galactic Nuclei, 2nd. eds. D. E. Osterbrock, & G. J. Ferland (Sausalito, CA: University Science Books)
Proga, D., & Kallman, T. R. 2004, ApJ, 616, 688
Reichard, T. A., Richards, G. T., Hall, P. B., et al. 2003, AJ, 126, 2594
Rudy, R. J., Stocke, J. T., & Foltz, C. B. 1985, ApJ, 288, 531
Sameshima, H., Kawara, K., Matsuoka, Y., et al. 2011, MNRAS, 410, 1018
Schlegel, D. J., Finkbeiner, D. P., & Davis, M. 1998, ApJ, 500, 525
Schneider, D. P., Richards, G. T., Hall, P. B., et al. 2010, AJ, 139, 2360
Storey, P. J., & Hummer, D. G. 1995, MNRAS, 272, 41
Tolea, A., Krolik, J. H., & Tsvetanov, Z. 2002, ApJ, 578, L31
Tremaine, S., Gebhardt, K., Bender, R., et al. 2002, ApJ, 574, 740
Trump, J. R., Hall, P. B., Reichard, T. A., et al. 2006, ApJS, 165, 1
Tsuzuki, Y., Kawara, K., Yoshii, Y., et al. 2006, ApJ, 650, 57
Vanden Berk, D. E., Richards, G. T., Bauer, A., et al. 2001, AJ, 122, 549
Véron-Cetty, M.-P., Joly, M., & Véron, P. 2004, A&A, 417, 515
Vestergaard, M., & Wilkes, B. J. 2001, ApJS, 134, 1
Wang, T., Dai, H., & Zhou, H. 2008, ApJ, 674, 668
Wang, T., Zhou, H., Yuan, W., et al. 2009, ApJ, 702, 851
Weymann, R. J., Morris, S. L., Foltz, C. B., & Hewett, P. C. 1991, ApJ, 373, 23
Wills, B. J., Netzer, H., & Wills, D. 1985, ApJ, 288, 94
York, D. G., Adelman, J., Anderson, J. E., Jr., et al. 2000, AJ, 120, 1579
Zhang, S., Wang, T.-G., Wang, H., et al. 2010, ApJ, 714, 367